Conference on Modelling Fluid Flow (CMFF'25)
The 19th International Conference on Fluid Flow Technologies
Budapest, Hungary, August 26-August 29, 2025

PIPE FLOW ANALOGY IN A PLANAR MASS-SPRING-DAMPER SYSTEM

Róbert ROCHLITZ[1], Bendegúz D. BAK[2]

[1] Corresponding Author. Department of Fluid Mechanics, Faculty of Mechanical Engineering, Budapest University of Technology and Economics. Bertalan Lajos u. 4 - 6, H-1111 Budapest, Hungary. E-mail: rochlitzr@edu.bme.hu
[2] Department of Fluid Mechanics, Faculty of Mechanical Engineering, Budapest University of Technology and Economics. E-mail: bak.bendeguz@gpk.bme.hu

ABSTRACT

We construct a chain oscillator whose block masses are connected by linear springs and linear dampers and each block is capable of 2D movement. This capability for moving in two directions gives rise to geometric nonlinearity in both the spring and the damping forces.

We investigate the behaviour of the planar system for initial conditions resulting in both linear and nonlinear response. The oscillator chain will be subjected to simultaneous forcing of each of its block masses, whose results will be compared for different forcing magnitude and parametrisations of the system.

The mean positions of the planar oscillator's block masses are compared to the velocity fields arising in simple fluid flows in pipes. It is demonstrated that for certain parametrisations of the oscillator, the model can reproduce the velocity profiles of real pipe flows. In particular, the mean position of the masses follows a quadratic profile for forcing similar to the constant pressure gradient which facilitates Poiseuille flows.

Keywords: flow modelling, nonlinear dynamics, pipe flow

NOMENCLATURE

E	[−]	energy
c	[−]	damping
f_0	[−]	scaling parameter of the forcing
k	[−]	spring stiffness
l	[−]	free spring length
m	[−]	element mass
n	[−]	number of elements
p	[−]	fitted polynomial
t	[−]	time
x	[−]	horizontal position
y	[−]	vertical position
R^2	[−]	fit quality
$\mathbf{F}_\mathrm{d}$	[−]	damping force
$\mathbf{F}_\mathrm{f}$	[−]	forcing
$\mathbf{F}_\mathrm{s}$	[−]	spring force
$\mathbf{r}$	[−]	position vector
σ	[−]	scaling parameter

Subscripts and Superscripts

i, j	indices
$\bar{}$	temporal average

1. INTRODUCTION

The mechanistic turbulence (MT) model depicted in Fig. 1 was first introduced as an attempt to explain Richardson's eddy hypothesis [1] with a mechanical system. It consists of a binary tree of masses connected by springs, with damping between the blocks that constitute the two bottom levels. For gradually decreasing block masses connected by with linear springs it is able to exhibit an energy distribution across its scales, that is similar to the turbulent energy spectrum [2] derived by Kolmogorov [3] for 3D homogeneous isotropic turbulence. This turbulent energy cascade is enabled by irreversible transfer of energy from the largest scales of the turbulent flow towards the smallest, dissipative scales.

By introducing cubic nonlinearity to the springs connecting the last two levels of the binary tree (as seen in Fig. 1), the model was found to be capable of efficient targeted energy transfer (TET) towards the nonlinear, dissipative elements for both impulsive and harmonic excitation of the top blocks which have the largest masses [4]. This irreversible transfer of energy results in efficient dissipation [5], and has been used for both vibration absorption [6, 7] and energy harvesting [8]. Thus, the TET found in the nonlinear MT model produces an energy cascade from the largest mass scales to the smallest mass scales, where the energy is ultimately dissipated. This process is chaotic for impulsive excitation of the largest block masses. The model also has chaotic bands [4], which are frequency regions where harmonic excitation induces chaos in the system according to Chen et al. [9].

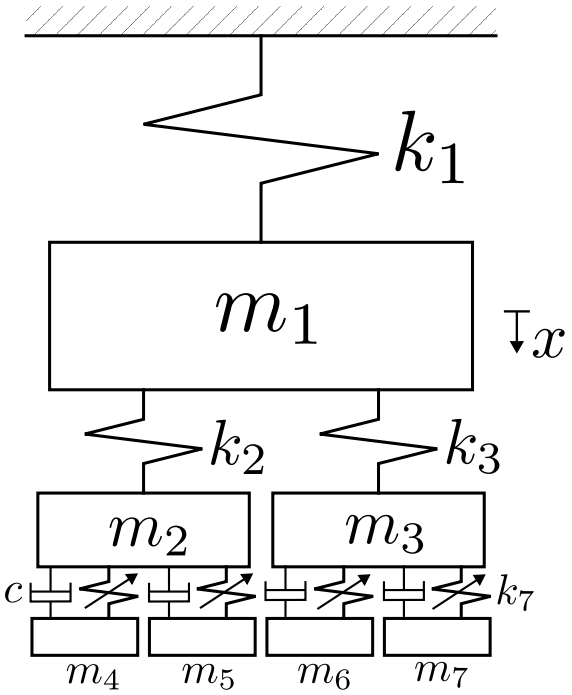

Figure 1. Mechanistic turbulence model with $n = 3$ levels, and springs with cubic nonlinearity between the last two levels

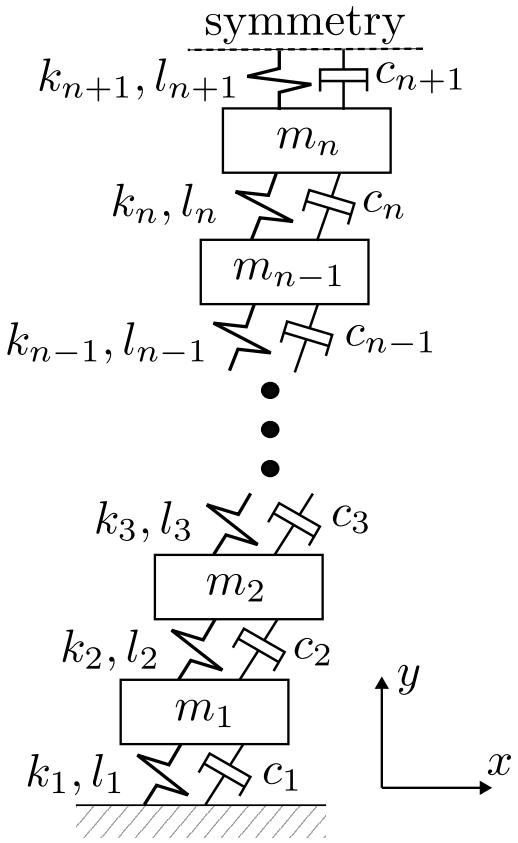

Figure 2. General form of the planar oscillator with a wall and a symmetry boundary condition

Despite its success in nonlinear dynamics, the MT model so far had only limited applications in modelling fluid mechanics. The aim of this paper is to introduce a planar version of the MT model that features geometric nonlinearity as shown in Fig. 2. We show that this planar oscillator is capable of expressing certain features of simple fluid flows – namely the velocity profile of a Poiseuille flow with constant pressure gradient [10] – while being able to exhibit nonlinear phenomena found in the MT model as well.

2. MODEL DESCRIPTION

The planar oscillator shown in Fig. 2 consists of a chain oscillator with n blocks connected by springs and dampers with linear characteristics. A wall and a symmetry boundary condition is applied at the bottom and the top blocks, respectively. The m_i masses, c_i dampings, k_i stiffnesses, and l_i spring lengths follow the relations

$$\begin{aligned} m_i &= \sigma^{n-i}, & i &= 1,\dots,n \\ c_i &= 0.01, & i &= 1,\dots,n+1 \\ k_i &= 1, & i &= 1,\dots,n+1 \\ l_i &= \sigma^{n+1-i} & i &= 1,\dots,n+1, \end{aligned} \tag{1}$$

where $\sigma > 0$ is a scaling parameter. Note that the quantities introduced throughout this paper are taken to be dimensionless, as it focuses on the qualitative behaviour of the system. The power laws and the light damping in Eq. (1) are introduced to obtain a parametrisation in line with the MT model that is described in [2, 4].

The elements of the chain oscillator are the block masses. These are treated as point masses, i.e. they have no rotational degrees of freedom. The equation of motion determining the $\mathbf{r}_i = (x_i, y_i)$ position of element $i = 1,\dots,n$ is

$$m_i\ddot{\mathbf{r}}_i = \mathbf{F}_{\mathrm{d},i,i+1} - \mathbf{F}_{\mathrm{d},i-1,i} + \mathbf{F}_{\mathrm{s},i,i+1} - \mathbf{F}_{\mathrm{s},i-1,i} + \mathbf{F}_{\mathrm{f},i}, \tag{2}$$

where $\mathbf{F}_{\mathrm{d},i,j}$ and $\mathbf{F}_{\mathrm{s},i,j}$ are the damping and spring forces acting on element i, defined as

$$\begin{aligned} \mathbf{F}_{\mathrm{d},i,j} &= \frac{\left(\mathbf{r}_j - \mathbf{r}_i\right)\cdot\left(\dot{\mathbf{r}}_j - \dot{\mathbf{r}}_i\right)}{\left\|\mathbf{r}_j - \mathbf{r}_i\right\|^2} c_i\left(\mathbf{r}_j - \mathbf{r}_i\right), \\ \mathbf{F}_{\mathrm{s},i,j} &= \left(1 - \frac{l_i}{\left\|\mathbf{r}_j - \mathbf{r}_i\right\|}\right) k_i\left(\mathbf{r}_j - \mathbf{r}_i\right), \end{aligned} \tag{3}$$

and $\mathbf{F}_{\mathrm{f},i}$ is the forcing applied to element i. This means that the damping force $\mathbf{F}_{\mathrm{d},i,j}$ and the spring force $\mathbf{F}_{\mathrm{s},i,j}$ act only along the line connecting the elements i and j.

Element $i = 1$ is connected to a wall, i.e., the boundary condition

$$\mathbf{r}_0(t) = \mathbf{0}, \tag{4}$$

is applied. At the other end of the chain oscillator a symmetry boundary condition is applied to element

n, resulting in

$$\begin{aligned} x_{n+1}(t) &= x_n(t), \\ y_{n+1}(t) &= 2\sum_{i=1}^{n} l_i + l_{n+1} - y_n(t). \end{aligned} \tag{5}$$

This means that the position of the masses m_n and m_{n+1} are reflections of each other with respect to the symmetric boundary.

The total energy of the system is defined as the sum of the potential energy of the springs and the kinetic energy of the blocks, i.e.,

$$\begin{aligned} E(t) = &\sum_{i=1}^{n+1} \frac{k_i}{2(1+\delta_{n+1,i})} \left(\|\mathbf{r}_i(t) - \mathbf{r}_{i-1}(t)\| - l_i\right)^2 \\ &+ \frac{1}{2}\sum_{i=1}^{n} m_i \|\dot{\mathbf{r}}_i(t)\|^2 , \end{aligned} \tag{6}$$

where $\delta_{n+1,i}$ is the Kronecker delta.

3. SIMULATION RESULTS

The equation of motion (2) of the planar oscillator was solved numerically with boundary conditions (4)-(5) for different values of the σ scaling parameter introduced in Eq. (1). While the qualitative behaviour of the system is not sensitive for the particular value of σ, different issues arise upon choosing a too high or low value significantly increasing the computational time. For high values (when σ is close to 1) the system requires a large number of blocks to include a wide range of mass scales. For lower values of the scaling parameter ($\sigma \leq 0.5$) simulating more than $n \approx 10$ levels is computationally challenging, because the proportion of the largest and the smallest mass and length scales becomes large enough that the simulation requires much finer time discretisation, leading to increased computational time.

3.1. Impulsive excitation

The planar oscillator is considered with $n = 30$ levels and $\sigma = 0.8$, as this combination of parameters was found to provide a sufficiently broad range of mass scales in Eq. (1) without adversely affecting the computation accuracy and time.

The initial conditions providing the impulsive excitation for the simulations are given by

$$\begin{aligned} \mathbf{r}_i(0) &= \begin{bmatrix} 0 \\ 1 \end{bmatrix} \sum_{j=1}^{i} l_j, \quad i = 0, \ldots, n, \\ \dot{\mathbf{r}}_i(0) &= 0, \quad i = 0, \ldots, n-1, \\ \dot{\mathbf{r}}_n(0) &= \begin{bmatrix} 0 \\ 1 \end{bmatrix} \text{ or } \begin{bmatrix} 1 \\ 0 \end{bmatrix}, \end{aligned} \tag{7}$$

meaning that every element starts in equilibrium and only element n has nonzero initial velocity. As this section considers impulsive excitations, no forcing was applied to the system, i.e.

$$\mathbf{F}_{\mathrm{f},i} = \mathbf{0}, \quad i = 1, \ldots, n. \tag{8}$$

As indicated in Eq. (7), two cases are considered with the same initial velocity magnitude for element n. In the first one, the initial velocity $\dot{\mathbf{r}}_n(0)$ has a zero x component, i.e.,

$$\dot{\mathbf{r}}_n(0) = \begin{bmatrix} 0 \\ 1 \end{bmatrix}. \tag{9}$$

This results in linear behaviour, as the only source of nonlinearity in the planar oscillator is the geometric nonlinearity facilitated by movement in the x direction. The second case has a nonzero x component and a zero y component, i.e.,

$$\dot{\mathbf{r}}_n(0) = \begin{bmatrix} 1 \\ 0 \end{bmatrix}, \tag{10}$$

introducing nonlinear effects.

Interestingly, the linear case given by the initial condition in Eq. (9) provides a stronger dissipation of the total energy $E(t)$ compared to the nonlinear case given by Eq. (10), as seen in Fig. 3. This means that the geometric nonlinearity did not facilitate the efficient energy dissipation seen in some nonlinear dynamical systems [5, 6, 7, 8].

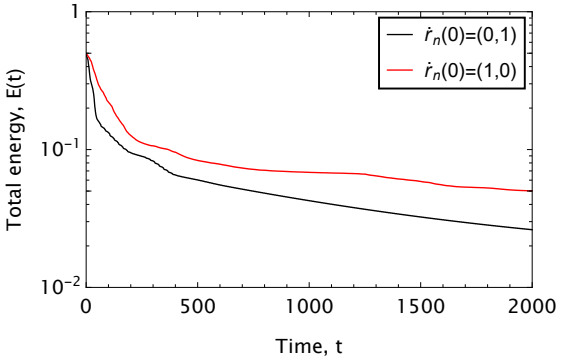

Figure 3. Total energy over time with impulsive excitation given by the initial conditions in Eqs. (7)**-**(10)

3.2. Poiseuille flow

As a next step, the equation of motion of the planar oscillator was solved with a forcing similar to those driving Poiseuille flows [10]. The investigations are carried out for three different values of the scaling parameter σ, which are shown in Tab. 1. along with the number of blocks in the oscillator and the chosen forcing parameters f_0.

Table 1. Number of blocks in the oscillator for the different values of the scaling parameter σ

σ	n
0.5	10
0.8	30
0.9	30

Poiseuille flows arise as a result of a constant pressure gradient [10]. Assuming constant density of the fluid, this results in a force acting on any fi-

nite fluid element proportional to the fluid element's mass. Analogously to Poiseuille flows, the static force applied to element i is defined here as

$$\mathbf{F}_{\mathrm{f},i}(t) = \begin{bmatrix} f_0 m_i \\ 0 \end{bmatrix}, \quad i = 0, \ldots, n, \tag{11}$$

where f_0 is the parameter determining the strength of forcing. In this section, possible values of 0.01, 0.1, and 1 are examined.

This time the initial conditions for the equation of motion (2) were set as

$$\begin{aligned} \mathbf{r}_i(0) &= \begin{bmatrix} 0 \\ 1 \end{bmatrix} \sum_{j=1}^{i} l_j, \quad i = 0, \ldots, n, \\ \dot{\mathbf{r}}_i(0) &= 0, \quad i = 0, \ldots, n, \end{aligned} \tag{12}$$

which means that every spring is initially relaxed and every element starts at rest.

The displacement solutions $x(t)$, $y(t)$ were calculated, then the total energy of the system was also obtained using Eq. (6). The resulting time histories of the total energy $E(t)$ are shown in Fig. 4. for some values of f_0 and σ. In every examined case, Fast Fourier Transform shows that the total energy has harmonic behaviour, with the exception of the case $\sigma = 0.5$ and $f_0 = 0.01$, which has the smallest energy content. In that case, additional modes are present in the $\mathbf{r}_n(t)$ solution compared to every other investigated case.

The oscillations of the total energy $E(t)$ are caused by the fact that the potential energy corresponding to the $\mathbf{F}_{\mathrm{f},i}$ static forces is not taken into account when calculating $E(t)$ according to Eq. (6).

The horizontal displacements exhibit the same qualitative behaviour as $E(t)$. For instance, the horizontal displacement $x_n(t)$ of the block at the symmetry boundary is shown in Fig. 5.

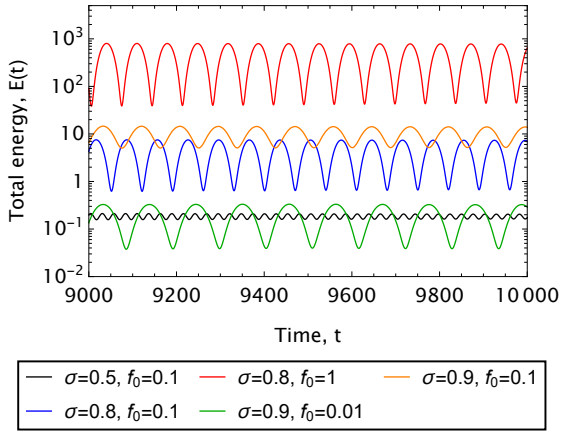

Figure 4. The total energy $E(t)$ of the system as a function of time for some values of σ, n, and f_0 according to Tab. 1, forcing according to Eq. (11), and ICs given in Eq. (12)

The vertical displacement $y_n(t)$ of the block at the symmetry boundary is shown in Fig. 6. for some

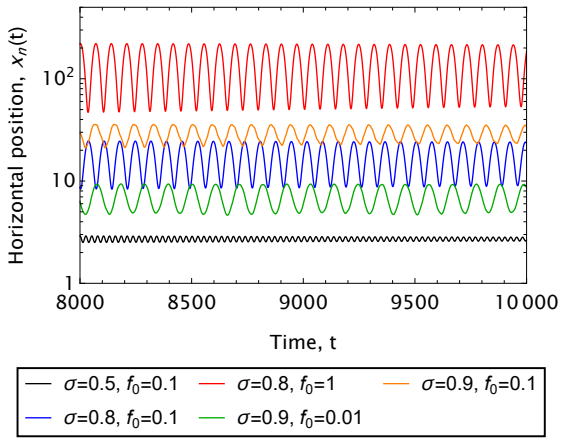

Figure 5. The horizontal displacement $x_n(t)$ of the block at the symmetry boundary as a function of time for some values of σ, n, and f_0 according to Tab. 1, forcing according to Eq. (11), and ICs given in Eq. (12)

of the examined values of σ and f_0. We observed that the frequencies of the components in $y_n(t)$ change as f_0 varies for each value of σ. Nonetheless, for $\sigma = 0.5$ and $\sigma = 0.9$ the emergent behaviour remains the same. In contrast, $y_n(t)$ for $\sigma = 0.8$ shows drastically different behaviour for different f_0 values. Thus we conclude that unlike the horizontal position $x_n(t)$, the qualitative behaviour of the vertical displacements of the blocks are strongly dependent on the parametrisation of the system and the magnitude of the forcing.

For Poiseuille flows in a circular pipe or between two plates with constant cross section and pressure gradient, the velocity profile is a second degree polynomial of the distance from the pipe axis [10]. As the Hagen-Poiseuille equation is a second order differential equation for the flow velocity, similarly to the equation of motion (2) for the displacement of the blocks, it is reasonable to test a second degree polynomial $p(y)$ fit to the $(\bar{x}_i, \bar{y}_i)$ mean displacement of the blocks.

An example of this is shown in Fig. 7 with $f_0 = 0.1$ for each value of the scaling parameter σ given in Tab. 1. Similarly good quality fits were found for the remaining combinations of σ and f_0. This result is non-trivial, as the second degree polynomials of the mean displacements arise despite the fact that the forcing given in Eq. (11) is an exponential function of the block index.

Tabs. 2-4 show the best fit found for the examined cases by minimising the root-mean-square of the $x_i - p(y_i)$ differences. The table suggests a trend towards decreasing R^2 values as the f_0 forcing parameter is increased, regardless of the value of σ. This observation, along with the relatively large drop in R^2 for $f_0 = 1$ suggests that for sufficiently large values of the forcing parameter, the system undergoes a transition whereby the $\bar{x}_i$ mean horizontal displace-

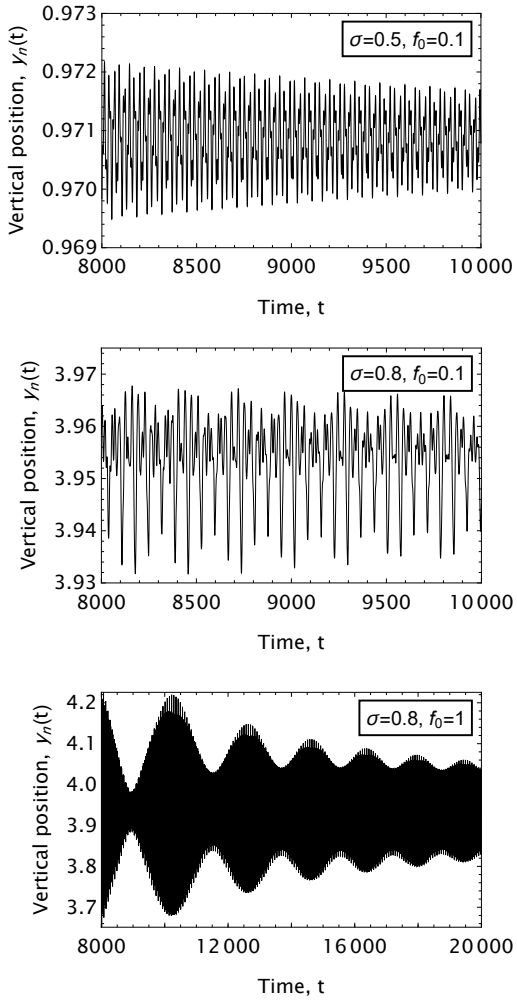

Figure 6. The vertical displacement $y_n(t)$ of the block at the symmetry boundary as a function of time for some values of σ, n, and f_0 according to Tab. 1, forcing according to Eq. (11), and ICs given in Eq. (12)

ments lose their quadratic characteristic.

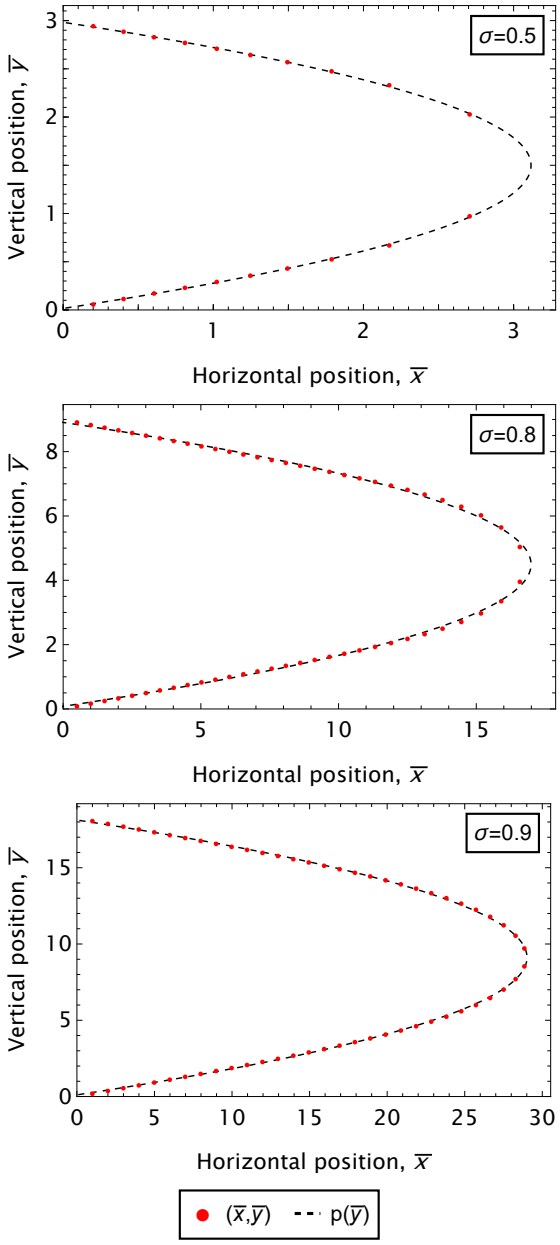

Figure 7. The $(\bar{x}_i, \bar{y}_i)$ mean displacement of the elements and the fitted second order polynomial for $f_0 = 0.1$, with σ and n according to Tab. 1, forcing according to Eq. (11), and ICs given in Eq. (12)

Table 2. Second degree polynomials fitted to the $(\bar{y}_i, \bar{x}_i)$ dataset for different values of the f_0 forcing parameter, with $\sigma = 0.5$

f_0	Fitted polynomial	R^2 value
0.01	$-0.380y^2 + 1.14y - 0.00102$	0.9999
0.1	$-1.42y^2 + 4.25y - 0.0669$	0.9993
1	$-10.3y^2 + 30.7y - 1.23$	0.9965

Table 3. Second degree polynomials fitted to the $(\bar{y}_i, \bar{x}_i)$ dataset for different values of the f_0 forcing parameter, with $\sigma = 0.8$

f_0	Fitted polynomial	R^2 value
0.01	$-0.188y^2 + 1.69y + 0.000403$	0.9997
0.1	$-0.872y^2 + 7.84y - 0.634$	0.9979
1	$-7.03y^2 + 63.2y - 12.2$	0.9864

Table 4. Second degree polynomials fitted to the $(\bar{y}_i, \bar{x}_i)$ dataset for different values of the f_0 forcing parameter, with $\sigma = 0.9$

f_0	Fitted polynomial	R^2 value
0.01	$-0.0835y^2 + 1.52y + 0.0608$	0.9995
0.1	$-0.357y^2 + 6.52y - 0.705$	0.9994
1	$-2.81y^2 + 51.3y - 12.9$	0.9961

4. SUMMARY

A planar oscillator chain was introduced with geometric nonlinearity. The behaviour of this oscillator was tested for initial conditions resulting in linear and nonlinear behaviour (see Eqs. (9) and (10), respectively) for impulsive excitations. It was found that the vertical initial velocity resulting in linear behaviour is somewhat more efficient at dissipating the initial energy of the system.

A constant forcing was introduced, analogously to the Poiseuille flow with a constant pressure gradient. The forced system was examined for three different values of the scaling parameter σ, each with three different f_0 forcing parameters. The total energy and the horizontal displacement of the block at the symmetry boundary showed harmonic behaviour over time in all cases, except for $\sigma = 0.5$ and $f_0 = 0.01$.

The vertical displacement of the blocks exhibited massive qualitative changes for the investigated combinations of σ and f_0 indicating high sensitivity of the system to these parameters. Yet, the oscillator is capable of reproducing the quadratic profile seen in Poiseuille flows regardless of the value of σ and f_0.

In future works, we plan to compare the results of constant forcing to Poiseuille flows quantitatively as well, and extend the analysis by comparing the behaviour of the planar oscillator chain during harmonic forcing with flows induced by an oscillating pressure gradient.

ACKNOWLEDGEMENTS

The project supported by the Doctoral Excellence Fellowship Programme (DCEP) is funded by the National Research Development and Innovation Fund of the Ministry of Culture and Innovation and the Budapest University of Technology and Economics.

The research reported in this paper is part of project no. TKP-6-6/PALY-2021. Project no. TKP-6-6/PALY-2021 has been implemented with the support provided by the Ministry of Culture and Innovation of Hungary from the National Research, Development and Innovation Fund, financed under the TKP2021-NVA funding scheme.

This work has been supported by the Hungarian National Research, Development and Innovation Fund under contract NKFI K 137726.

One of the authors, Bendegúz D. Bak has also been supported by the János Bolyai Research Scholarship of the Hungarian Academy of Sciences.

REFERENCES

[1] Richardson, L. F., 1922, *Weather Prediction by Numerical Process*, Cambridge University Press.

[2] Kalmár-Nagy, T., and Bak, B. D., 2019, "An intriguing analogy of Kolmogorov's scaling law in a hierarchical mass–spring–damper model", *Nonlinear Dynamics*, Vol. 95 (4), pp. 3193–3203.

[3] Kolmogorov, A. N., 1941, "The local structure of turbulence in incompressible viscous fluid for very large Reynolds numbers", *Dokl. Akad. Nauk SSSR*, JSTOR, Vol. 30, pp. 301–305.

[4] Bak, B. D., Rochlitz, R., and Kalmár-Nagy, T., 2023, "Energy transfer mechanisms in binary tree-structured oscillator with nonlinear energy sinks", *Nonlinear Dynamics*, Vol. 111 (11), pp. 9875–9888.

[5] Vakakis, A. F., Gendelman, O. V., Bergman, L. A., McFarland, D. M., Kerschen, G., and Lee, Y. S., 2008, *Nonlinear Targeted Energy Transfer in Mechanical and Structural Systems*, Vol. 156, Springer Science & Business Media.

[6] Starosvetsky, Y., and Gendelman, O. V., 2009, "Vibration absorption in systems with a nonlinear energy sink: Nonlinear damping", *Journal of Sound and Vibration*, Vol. 324, pp. 916–939.

[7] Yang, K., Zhang, Y.-W., Ding, H., Yang, T.-Z., Li, Y., and Chen, L.-Q., 2017, "Nonlinear Energy Sink for Whole-Spacecraft Vibration Reduction", *Journal of Vibration and Acoustics*, Vol. 139 (2).

[8] Kremer, D., and Liu, K., 2014, "A nonlinear energy sink with an energy harvester: Transient responses", *Journal of Sound and Vibration*, Vol. 333 (20), pp. 4859–4880.

[9] Chen, J. E., Theurich, T., Krack, M., Sapsis, T., Bergman, L. A., and Vakakis, A. F., 2022, "Intense cross-scale energy cascades resembling "mechanical turbulence" in harmonically driven strongly nonlinear hierarchical chains of oscillators", *Acta Mechanica*, Vol. 233 (4), pp. 1289–1305.

[10] Drazin, P. G., and Riley, N., 2006, *The Navier-Stokes Equations: A Classification of Flows and Exact Solutions*, London Mathematical Society Lecture Note Series, Cambridge University Press.